

## Scaling of angiosperm xylem structure with safety and efficiency

UWE G. HACKE,<sup>1,3</sup> JOHN S. SPERRY,<sup>1</sup> JAMES K. WHEELER<sup>1</sup> and LAURA CASTRO<sup>2</sup>

<sup>1</sup> Department of Biology, University of Utah, Salt Lake City, UT 84112, USA

<sup>2</sup> Unidad de Anatomía, Fisiología y Genética Forestal, Escuela Técnica Superior de Ingenieros de Montes, Universidad Politécnica de Madrid, Ciudad Universitaria s/n, 28040 Madrid, Spain

<sup>3</sup> Corresponding author (hacke@biology.utah.edu)

Received June 9, 2005; accepted September 28, 2005; published online March 1, 2006

**Summary** We tested the hypothesis that greater cavitation resistance correlates with less total inter-vessel pit area per vessel (the pit area hypothesis) and evaluated a trade-off between cavitation safety and transport efficiency. Fourteen species of diverse growth form (vine, ring- and diffuse-porous tree, shrub) and family affinity were added to published data predominately from the Rosaceae (29 species total). Two types of vulnerability-to-cavitation curves were found. Ring-porous trees and vines showed an abrupt drop in hydraulic conductivity with increasing negative pressure, whereas hydraulic conductivity in diffuse-porous species generally decreased gradually. The ring-porous type curve was not an artifact of the centrifuge method because it was obtained also with the air-injection technique. A safety versus efficiency trade-off was evident when curves were compared across species: for a given pressure, there was a limited range of optimal vulnerability curves. The pit area hypothesis was supported by a strong relationship ( $r^2 = 0.77$ ) between increasing cavitation resistance and diminishing pit membrane area per vessel ( $A_p$ ). Small  $A_p$  was associated with small vessel surface area and hence narrow vessel diameter ( $D$ ) and short vessel length ( $L$ )—consistent with an increase in vessel flow resistance with cavitation resistance. This trade-off was amplified at the tissue level by an increase in xylem/vessel area ratio with cavitation resistance. Ring-porous species were more efficient than diffuse-porous species on a vessel basis but not on a xylem basis owing to higher xylem/vessel area ratios in ring-porous anatomy. Across four orders of magnitude, lumen and end-wall resistivities maintained a relatively tight proportionality with a near-optimal mean of 56% of the total vessel resistivity residing in the end-wall. This was consistent with an underlying scaling of  $L$  to  $D^{3/2}$  across species. Pit flow resistance did not increase with cavitation safety, suggesting that cavitation pressure was not related to mean pit membrane porosity.

*Keywords:* hydraulic conductivity, trade-offs, vulnerability curves, water transport, wood structure, xylem anatomy, xylem cavitation.

### Introduction

The xylem conduit network supplies a transpiration stream

that is under significant negative pressure. The conduits must protect this stream against rupture by cavitation—the abrupt transition from metastable liquid to gas phase (Zimmermann 1983). At the same time that the xylem must be safe from cavitation, it must have a sufficiently low resistance to water flow to minimize the transpiration-induced drop in negative pressure. Most plants regulate their canopy xylem pressures through adjustments in stomatal conductance and leaf area (Meinzer and Grantz 1990, Hacke et al. 2000, Hubbard et al. 2001). Consequently, the lower the transport resistance, the more water can flow to the canopy under a given pressure gradient, and the greater the capacity for carbon uptake. The lower the xylem resistivity is on a cross-sectional area basis, the greater the photosynthetic profit per xylem investment.

This paper focuses on isolating the structural requirements for safety on the one hand, and transport efficiency on the other. This allows us to identify mechanisms that may limit the simultaneous optimization of safety and transport efficiency. This potential trade-off is different from the xylem safety versus xylem investment conflict analyzed previously (Hacke et al. 2001a, 2004). In those studies, increasing safety from cavitation corresponded with increased investment in conduit wall volume per conduit volume as predicted to withstand implosion by greater negative pressure. This translated to a minimum wood density required to reinforce conduit walls—a construction cost that increased with the capacity to withstand negative pressure. The related conflict, which is the focus of this paper, is whether increased cavitation safety requires decreased hydraulic efficiency.

A safety versus efficiency trade-off has long been proposed (Zimmermann and Brown 1977, Carlquist 1988), but the evidence is ambiguous (Tyree et al. 1994, Choat et al. 2005). If there is a trade-off, plants with more negative cavitation pressure might show an increase in the resistivity of their functional xylem and a decrease in vessel size. This is seen in some data sets (Martinez-Vilalta et al. 2002), but the relationship can be statistically weak (Tyree et al. 1994, Pockman and Sperry 2000). Other data sets show no relationship at all (Hacke and Sperry 2001, Jacobsen et al. 2005).

Adding to the ambiguity is that the mechanism of cavitation by water stress is not linked in any self-evident way to vessel

size (diameter and length), which has a strong influence on xylem flow resistance. There is considerable evidence that cavitation is caused by air being drawn into water-filled xylem conduits by negative pressure and that the most important sites of this air-seeding are the inter-conduit pits (Crombie et al. 1985, Sperry and Tyree 1988, 1990, Jarbeau et al. 1995). These pits connect adjacent conduits to allow water flow and they also act as safety valves to block the spread of gas from embolized conduits. In inter-vessel membranes, the pit is sealed against air entry by capillary forces at the narrow pores of the pit membrane. Excessively negative pressure during water stress, however, can pull air across the pit valves and cause cavitation in adjacent water-filled conduits. It is unclear whether the pit properties that dictate safety from cavitation also constrain vessel length and diameter, and thus the overall resistivity of the conduit network.

In an attempt to unravel the link between pit function and xylem flow resistance, we have previously modeled the air-seeding and hydraulic properties of pits (Hacke et al. 2004, Sperry and Hacke 2004). A major assumption of the model as applied to homogeneous pit membranes of angiosperm vessels (to distinguish from the torus-margo organization in gymnosperms), was that mean porosity of the cellulosic mesh of the pit membrane covaried with the maximum pore size of the membrane and that all pit membranes in a vessel were identical. The maximum membrane pore size in a vessel is critical because the relatively weak capillary forces at this pore set the air-seeding pressure for the entire vessel. The bigger this maximum pore, the more vulnerable is the vessel to cavitation by capillary failure (assuming the membrane does not air-seed by rupture or extensive plastic yielding). According to our assumptions, a vessel could achieve greater safety from air-seeding only by having a denser pit membrane mesh with reduced mean porosity. This would result in a strong trade-off between increasing safety from air-seeding (set by a decline in maximum membrane pore size) and increasing flow resistance through a pit (determined by declining mean porosity of the pit membrane). We refer to this as the pit resistance hypothesis for a safety versus efficiency conflict at the pit level.

Recent estimates of pit membrane resistance do not support this hypothesis. Instead of a strong increase in pit resistance (on a membrane area basis) with increasing safety from cavitation, there was no relationship (Wheeler et al. 2005). Furthermore, measured resistances were considerably greater than model predictions, indicating an average membrane porosity far smaller than modeled. These results agree with some experimental results suggesting an average membrane pore size much smaller than the size predicted to air-seed at the cavitation pressure (Choat et al. 2003, but see Jarbeau et al. 1995). The data of Wheeler et al. (2005) suggest that average pore size, though variable, does not correlate well with the largest membrane pore per vessel that limits safety from air-seeding. This result leaves open the question of what features of pit and vessel structure influence the largest membrane pore per vessel.

A possible answer to this question is that it is the total number, or collective membrane area, of pits in a vessel that influ-

ences the largest pore per vessel (Hargrave et al. 1994, Choat et al. 2005). Our previous survey showed a strong inverse relationship between increasing total pit membrane area per vessel and decreasing safety from cavitation. The greater the pit area in the vessel, the larger the maximum pore size for the vessel (Wheeler et al. 2005). This conclusion suggests there is an element of probability in the safety of a vessel from cavitation. Adding more pits to a vessel compromises its safety from cavitation because the more pits there are, by chance the greater will be the single largest pore diameter in the vessel. The average porosity of the pit membranes and their resistance on an area basis, however, would not necessarily change. This pit area hypothesis provides a basis for a safety versus efficiency trade-off because a limitation on vessel pit area can also limit vessel size and flow resistance (Wheeler et al. 2005).

The results of Wheeler et al. (2005) were from 16 species, 11 of which were members of the Rosaceae (Table 2). The emphasis on the Rosaceae was intended to minimize qualitative differences in pit membrane structure across lineages, and so to maximize the probability of detecting safety-related variation in pit properties. However, this sampling prevented the widest possible variation in vessel sizes and cavitation resistance. Furthermore, no family bias was detected in the results, suggesting the observed trends may cut across phylogenetic groups.

The present paper adds 14 species to the data set of Wheeler et al. (2005), the new species were chosen for extremes of vessel size and cavitation pressure to more effectively determine scaling relationships between the structure and function of vessels (Table 1). Family affinities were diverse, but with the exception of two species, they were families without vested pitting. Vestures could modify some structure–function relationships (Choat et al. 2004) and a systematic comparison was outside the scope of this project. The species were chosen to represent large vessels of ring-porous trees (six species) and vines (one species) at one extreme, and narrower vessels of diffuse-porous trees and shrubs (seven species) on the other. The goals were (1) to determine if the inclusion of more diverse vessel sizes and safeties confirmed the pit area hypothesis over the pit resistance hypothesis; (2) to evaluate the implications of the hypothesis for a safety versus efficiency trade-off; and (3) to explore the ramifications of the ring-porous versus diffuse-porous vessel organizations with respect to the safety versus efficiency conflict.

## Materials and methods

Our methods were nearly identical to those described by Wheeler et al. (2005) and only a brief summary is provided here except for descriptions unique to the 14 species added to the existing data set.

### *Plant material*

Studied plants (Table 1) represented different xylem types (diffuse-porous and ring-porous), growth forms (trees, shrubs and vines), ecosystems (from the abundant moisture in North Carolina to the aridity of the American Southwest) and leaf

Table 1. Study species, their figure symbols and measurements not shown in figures. The first five species are ring-porous and are designated by asterisked double capital symbols. Measurements represent the mean vessel size. Contact fraction is the fraction of vessel surface area contacting another vessel. Pit-field fraction is the fraction of inter-vessel contact occupied by pit membranes. The product of these two fractions gives the pit fraction ( $F_p$ ), the total pit area per vessel surface area. Length fraction is the portion of vessel length overlapping other vessels. The ratio  $L'/L = F_L$  is the length between end walls ( $L'$ ) per vessel length ( $L$ ). Grand means from a minimum of six stems per species  $\pm$  SE.

Species	Figure symbol	Contact fraction	Pit-field fraction	Length fraction	$L'/L = F_L$
<i>Carya glabra</i> (P. Mill.) Sweet (Juglandaceae)	CG*	0.07 $\pm$ 0.010	0.55 $\pm$ 0.044	0.17 $\pm$ 0.020	0.91 $\pm$ 0.010
<i>Fraxinus pennsylvanica</i> Marsh. (Oleaceae)	FP*	0.11 $\pm$ 0.009	0.55 $\pm$ 0.019	0.26 $\pm$ 0.022	0.87 $\pm$ 0.011
<i>Morus alba</i> L. (Moraceae)	MA*	0.08 $\pm$ 0.013	0.61 $\pm$ 0.014	0.19 $\pm$ 0.022	0.91 $\pm$ 0.011
<i>Quercus gambelii</i> Nutt. (Fagaceae)	QG*	0.05 $\pm$ 0.019	0.30 $\pm$ 0.018	0.13 $\pm$ 0.019	0.94 $\pm$ 0.010
<i>Quercus prinus</i> L. (Fagaceae)	QP*	0.05 $\pm$ 0.014	0.39 $\pm$ 0.020	0.17 $\pm$ 0.019	0.91 $\pm$ 0.009
<i>Rhus trilobata</i> Nutt. (Anacardiaceae)	RT*	0.17 $\pm$ 0.015	0.52 $\pm$ 0.031	0.53 $\pm$ 0.026	0.74 $\pm$ 0.013
<i>Acer grandidentatum</i> Nutt. (Aceraceae)	Acg	0.30 $\pm$ 0.015	0.69 $\pm$ 0.016	0.50 $\pm$ 0.021	0.75 $\pm$ 0.011
<i>Arctostaphylos patula</i> E.L. Greene (Ericaceae)	Arp	0.10 $\pm$ 0.004	0.37 $\pm$ 0.020	0.21 $\pm$ 0.023	0.90 $\pm$ 0.011
<i>Ceanothus crassifolius</i> Torrey (Rhamnaceae)	Cec	0.10 $\pm$ 0.008	0.43 $\pm$ 0.025	0.18 $\pm$ 0.011	0.91 $\pm$ 0.005
<i>Ceanothus velutinus</i> Dougl. ex Hook. (Rhamnaceae)	Cev	0.19 $\pm$ 0.005	0.58 $\pm$ 0.033	0.33 $\pm$ 0.011	0.83 $\pm$ 0.005
<i>Larrea tridentata</i> (Sessé & Moc. ex DC.) Coville (Zygophyllaceae)	Lat	0.01 $\pm$ 0.001	0.40 $\pm$ 0.019	0.03 $\pm$ 0.003	0.99 $\pm$ 0.002
<i>Oxydendron arboreum</i> (L.) D.C. (Ericaceae)	Oxa	0.08 $\pm$ 0.006	0.30 $\pm$ 0.016	0.17 $\pm$ 0.013	0.91 $\pm$ 0.007
<i>Paxistima myrsinites</i> (Pursh) Raf. (Celastraceae)	Pam	0.13 $\pm$ 0.005	0.41 $\pm$ 0.023	0.21 $\pm$ 0.006	0.89 $\pm$ 0.003
<i>Pueraria montana</i> (Lour.) Merr. (Fabaceae)	Pum	0.16 $\pm$ 0.025	0.71 $\pm$ 0.010	0.38 $\pm$ 0.043	0.81 $\pm$ 0.021

phenologies (evergreens included: *Paxistima myrsinites*, *Cercocarpus ledifolius*, *Ceanothus velutinus*, *Larrea tridentata* and *Arctostaphylos patula*). Stems of *Carya glabra*, *Quercus prinus*, *Oxydendron arboreum* and the introduced vine *Pueraria montana* (Kudzu), were collected near Tryon, North Carolina in the Appalachian mountain foothills. *Ceanothus crassifolius* was collected from chaparral near Pepperdine University in Malibu, California. From these distant sites, the material was wrapped in plastic bags and shipped by overnight express to our laboratory in Salt Lake City, Utah. Stems of the remaining species were collected within a few hours drive of the laboratory and were similarly protected from desiccation

during transport. Additional species from the study of Wheeler et al. (2005) are listed in Table 2.

#### Cavitation pressure

Vulnerability curves documenting the decrease in hydraulic conductivity with negative pressure were measured on at least six stems per species by the centrifuge method (Alder et al. 1997) as in the previous study (Wheeler et al. 2005). Stems were flushed with measuring solution (20 mM KCl) under 100 kPa entry pressure to reverse native embolism before curve determination. The hydraulic head used to measure the conductivity was typically about 4 kPa in diffuse-porous stems and 1–2 kPa in stems with large vessels. A low pressure head in large and long-vessel species was essential to avoid instant refilling of embolized vessels cut open at both ends. Between conductivity measurements, stems were centrifuged to progressively more negative pressure in a custom-designed centrifuge rotor. Vulnerability curves showing the drop in conductivity with negative pressure were plotted for all six stems of a species and the collective species curve was fit with a Weibull function:

$$K/K_{\max} = e^{-(P/b)^c} \quad (1)$$

where  $K/K_{\max}$  is conductivity relative to the maximum in the absence of any reversible embolism,  $P$  is the absolute value of the negative pressure,  $b$  is a curve fitting parameter that corresponds to  $P$  at  $K/K_{\max} = 0.63$  and  $c$  is a curve-fitting parameter influencing the slope of the vulnerability curve. Table 3 defines major variables.

Some species for which stems older than one year had to be used (because of length limitations of current-year growth) exhibited the cavitation fatigue phenomenon (Hacke et al.

Table 2. Species from Wheeler et al. (2005) and figure symbols. The first 11 species are members of the Rosaceae.

Species	Figure symbol
<i>Amelanchier alnifolia</i> M. Roemer	Aa
<i>A. utahensis</i> Koehne	Au
<i>Cercocarpus ledifolius</i> Torr. & Gray	Cl
<i>C. montanus</i> Raf.	Cm
<i>Holodiscus dumosus</i> (Hook.) Heller	Hd
<i>Physocarpus malvaceus</i> (Greene) Kuntze	Pm
<i>Purshia tridentata</i> (Pursh) D.C.	Pt
<i>Rosa nutkana</i> C. Presl.	Rn
<i>Rubus leucodermis</i> Torr. & Gray	Rl
<i>R. parviflorus</i> Nutt.	Rp
<i>Sorbus scopulina</i> Greene	Ss
<i>Acer negundo</i> L. (Aceraceae)	An
<i>Salix exigua</i> Nutt. (Salicaceae)	Se
<i>Sambucus cerulea</i> Raf. (Adoxaceae)	Sc
<i>Vitis vinifera</i> L. (Vitaceae)	Vv

Table 3. Major variables with definition and units. Variables represent values for mean vessel size.

Symbol	Definition	Units
$A_p$	Total inter-vessel pit membrane surface area of vessel	$\text{mm}^2$
$A_v$	Total internal surface area of vessel	$\text{mm}^2$
$D$	Diameter corresponding to mean vessel $R_L$	$\mu\text{m}$
$F$	$R_L/R_W$ ratio	–
$F_L$	$L'/L$ ratio	–
$F_p$	Pit fraction = $A_p/A_v$	–
$K, K_{\max}$	Xylem conductivity, maximum conductivity	$\text{mm}^4 \text{MPa}^{-1} \text{s}^{-1}$
$K_{Xa}$	Xylem cross-sectional area conductivity	$\text{m}^2 \text{MPa}^{-1} \text{s}^{-1}$
$K_{Xa-\max}$	Maximum $K_{Xa}$ for non-embolized xylem	$\text{m}^2 \text{MPa}^{-1} \text{s}^{-1}$
$L$	Vessel length	cm
$L'$	Length between vessel end-walls	m
$R_C$	Vessel resistivity	$\text{MPa s mm}^{-4}$
$R_L$	Vessel lumen resistivity	$\text{MPa s mm}^{-4}$
$R_W$	Vessel end-wall resistivity	$\text{MPa s mm}^{-4}$
$R_{Ca}$	Vessel cross-sectional area resistivity	$\text{MPa s m}^{-2}$
$R_{Xa}$	Xylem cross-sectional area resistivity = $1/K_{Xa}$	$\text{MPa s m}^{-2}$
$r_W$	Resistance of one vessel end-wall	$\text{MPa s mm}^{-3}$
$r_P$	Pit membrane area resistance	$\text{MPa s m}^{-1}$

2001b). These species had high native embolism values and included ring-porous trees and some diffuse-porous species from drought-prone habitats. The fatigue phenomenon is the reduction in cavitation pressure in older xylem as a result of previous cavitation by drought (Hacke et al. 2001b), freezing (J.S. Sperry and L. Castro unpublished data; S.D. Davis, Pepperdine University, Malibu, USA, personal communication) and perhaps age itself (Sperry et al. 1991). The symptom of cavitation fatigue is highly vulnerable xylem localized to older growth rings. Dye perfusions show that this older xylem is embolized in the native condition and when refilled by flushing becomes re-embolized at very modest negative pressures (e.g.,  $-0.5$  MPa) in the laboratory. To avoid biasing estimates of the cavitation pressure of the functionally most important current-year xylem by including the older fatigued xylem, the  $K_{\max}$  of these species was scaled to  $K$  at  $-0.5$  MPa rather than the  $K$  after flushing (*A. patula*, *C. glabra*, *Fraxinus pennsylvanica*, *Paxistima myrsinites*, *Physocarpus malvaceus*, *Purshia tridentata* and *Rosa nutkana*). In *Larrea tridentata*, the  $K_{\max}$  was scaled to  $K$  at  $-1.5$  MPa because even the fatigued xylem was relatively resistant to cavitation in this extremely drought-adapted species.

Vulnerability curves of vines and ring-porous trees where we could avoid the fatigue artifact by using current-year growth (*Quercus gambelii*, *Q. prinus*, *P. montana*, *Morus alba* and *Rhus trilobata*) also tended to have a significant amount of native embolism and highly vulnerable vessels (e.g., Figures 1 and 2)—though less so than was the case with older stems. We did not scale these curves as described above because they were based solely on current-year xylem.

In a subset of large-vesseled and fatigue-prone species, we compared the centrifuge method with the air-injection technique as a check on the centrifuge method for large-vesseled species. Stems about 25 cm in length were sealed in a double-ended pressure chamber and the hydraulic conductivity

measured in between exposing the stem in the chamber to stepwise increases in air pressures (10 min per pressure). Vulnerability curves developed by this method show the drop in conductivity as a function of the air pressure and give the pressure range required to push the air into the xylem (Cochard et al. 1992, Sperry and Saliendra 1994). The air-injection curves should be equal and opposite to the centrifuge curves if air-seeding is the main cavitation mechanism. This test was done for *P. montana*, *R. trilobata*, *Q. gambelii* and *Quercus turbinella* (the latter species was not part of the extended study).

All comparisons of cavitation pressure and xylem structure were made between the species' mean value for each parameter. For this reason, it was necessary to represent the species' vulnerability curve with a single cavitation pressure. In the past, we have used either the pressure required to reduce  $K/K_{\max}$  to 0.5 ( $P_{50}$ ), or the mean cavitation pressure (e.g., Linton et al. 1998). The latter treats the vulnerability curve as a cumulative distribution of  $K$  with pressure and is the mean of that distribution. For species with nearly symmetrical sigmoidal or linear vulnerability curves,  $P_{50}$  and mean cavitation pressure are very similar. However, in this study, large-vesseled species typically had asymmetrical vulnerability curves characterized by an initial abrupt drop in conductivity with pressure followed by a tail where conductivity dropped more gradually (Figures 1 and 2). To better represent the cavitation pressure across curves of all shapes, we used the mean cavitation pressure for all species, including those previously represented by their  $P_{50}$  (Wheeler et al. 2005).

#### Xylem-area hydraulic resistivity

The hydraulic resistivity (pressure gradient per flow rate) of the sapwood of all species was measured and expressed relative to the sapwood area ( $R_{Xa}$ ). The  $R_{Xa}$  corresponds to  $1/K_{\max}$ , but is expressed on a functional xylem area basis. We switch between conductivities and resistivities because the latter are

additive in series and this facilitates the separation of vessel function into its components (e.g., Equation 2). The  $R_{Xa}$  had to be determined for segments longer than the longest vessels to include the influence of end-wall resistance. In most diffuse-porous stems,  $R_{Xa}$  could be directly measured in stem segments that were longer than the longest vessels (Wheeler et al. 2005). In these cases, six stems per species were measured. After the hydraulic measurements were completed, 0.05% safranin dye was siphoned through the segments (in stems > 1 year old) to mark the functional xylem. The area of functional xylem at the middle of the stem segment was measured with a light microscope and image analysis software. Resistivity was multiplied by this stained area to obtain  $R_{Xa}$  for each stem.

In long-vesseled species (*P. montana*, *F. pennsylvanica*, *C. glabra*, *M. alba*, *R. trilobata* and the two *Quercus* species), vessels were too long for direct measurements of  $R_{Xa}$ . Instead, we used the shortening technique to determine  $R_{Xa}$  (Sperry et al. 2005). Ten segments per species were selected, and the resistivity measured at segment lengths of 15, 5.1, 1.8 and 0.6 cm. In all species,  $R_{Xa}$  decreased significantly with decreasing segment length and as the percentage of open vessels without end walls increased (Sperry et al. 2005). The portion of open vessels was known from vessel length measurements (see below). The intercept of the resistivity versus percentage of open vessels relationship (at 0 cm segment length and 100% open vessels) gave an estimate of the resistivity of the vessel lumens. Sperry et al. (2005) observed that this intercept did not differ statistically from lumen resistivity ( $R_L$ ) calculated from measurements of vessel diameter and the Hagen-Poiseuille equation, and this was also found in our study species. For consistency across species, we used the Hagen-Poiseuille  $R_L$  estimate for all species (see next section). The other end of the regression line, the resistivity at 0% open vessels, gave our estimate of  $R_{Xa}$  for the xylem with fully intact vessels.

#### *Vessel diameter, Hagen-Poiseuille lumen resistivity and vessel density*

After completion of the  $R_{Xa}$  measurements, a subset of the same stems was used to measure vessel diameters, Hagen-Poiseuille lumen resistivity ( $R_L$ ) and vessel densities. These parameters were measured on transverse sections as described by Wheeler et al. (2005). For the diffuse-porous species, all six  $R_{Xa}$  stems were measured and for species requiring the stem-shortening method, four of the 10 stems were randomly chosen. Hagen-Poiseuille lumen resistivity was calculated for each vessel at the same temperature (and sap viscosity) at which  $R_{Xa}$  was measured experimentally. Because our purpose was to relate vessel structure to resistivity, we represented the mean diameter ( $D$ ) as the diameter corresponding to the mean  $R_L$  for each stem.

#### *Vessel length*

Vessel lengths ( $L$ ) were measured on a separate set of a minimum of five stems per species, but from the same batch and age as that used for the hydraulic measurements. The methods

have been described in detail (Sperry et al. 2005, Wheeler et al. 2005). Vessel length distributions are strongly short-skewed and the mean  $L$  used to represent a segment corresponded to the mean of the log-transformed vessel length distribution.

#### *Partitioning xylem resistivity into lumen and end-wall components*

Our purpose was to isolate the contribution of end-wall and lumen structure to the resistivity of intact vessels. To estimate these contributions, we assumed as in previous work (Wheeler et al. 2005) that, on average, lumen and end-wall components were arranged in series in the xylem network. If all the vessels of a stem are represented by an equal number of average-sized and average-resistance vessels, mean intact vessel resistivity ( $R_C$ ) is the sum of the mean lumen ( $R_L$ ) and end-wall ( $R_W$ ) resistivities:

$$R_C = R_L + R_W \quad (2)$$

We estimated  $R_C$  by multiplying  $R_{Xa}$  by mean vessel density, and  $R_L$  was estimated from vessel diameters and the Hagen-Poiseuille equation. The  $R_W$  was determined by subtraction.

#### *Partitioning $R_W$ into end-wall resistance and pit area resistance*

Based on the same analysis presented in Wheeler et al. (2005), we broke down the mean end-wall resistivity  $R_W$  into the mean resistance of a single end-wall ( $r_w$ ) based on the assumption that  $R_W$  (a resistivity) is the average end-wall resistance per average length between successive end-walls in series ( $L'$ ):

$$R_W = r_w / L' \quad (3)$$

where  $L'$  was calculated as mean vessel length ( $L$ ) minus the mean length of one of its two end-walls (Figure 1 in Wheeler et al. 2005). We estimated  $L'$  according to Wheeler et al. (2005), using the same stems measured for  $R_{Xa}$ .

End-wall resistance is a function of the number of pits in the end-wall and their individual resistances to flow. To estimate the resistance of a pit on its membrane area basis ( $r_p$ ), we assumed that all pits of an end-wall were in parallel, so that:

$$r_w = r_p / (A_p / 2) \quad (4)$$

where  $A_p$  is total area of inter-vessel pits, which is divided by 2 to obtain the pit area in one of the two vessel end-walls. This continues the assumption that all inter-vessel pits are between end walls. To the extent that there may be true lateral pitting between vessels (that is, two vessels meeting only at mid-length and separating), the end-wall pit area is overestimated, and hence our  $r_p$  values will be overestimates.

The  $A_p$  was estimated as the surface area of the average vessel ( $A_v = \pi DL$ ) multiplied by the mean fraction of the vessel surface area occupied by inter-vessel pits (the pit fraction,  $F_p$ ). The  $F_p$  was the product of the average vessel contact fraction and pit-field fraction, where the contact fraction is the fraction of the vessel surface area in contact with adjacent vessels and

the pit-field fraction is the fraction of the inter-vessel contact area occupied by pits. These fractions were measured according to Wheeler et al. (2005) on the same stems measured for  $R_{Xa}$ .

#### Summary equation for $R_{Ca}$ and $L$ versus $D$ scaling

To summarize how vessel structure influences vessel resistivity, we combined the essential parameters described above into a single summary equation for a species' mean vessel-area resistivity ( $R_{Ca} = R_C \times$  mean lumen cross-sectional area). This equation is derived in the appendix of Wheeler et al. (2005, Equation A8) and modified slightly here:

$$R_{Ca} = 6.06(\pi/A_p)^{4/5} \eta^{3/5} (F_p r_p / F_L)^{2/5} (F^{2/5} + F^{-3/5}) \quad (5)$$

where  $F = R_L/R_W$ , and is used for simplicity instead of the  $F_W = R_W/R_C$  fraction used in Wheeler et al. (2005, Equation A8). The  $F_L$  term =  $L'/L$ . A summary equation for  $L$  and  $D$  scaling was similarly obtained:

$$L = 0.125 \left( \frac{F r_p}{\eta F_p F_L} \right)^{1/2} (D)^{3/2} \quad (6)$$

Equation 6 was derived from Equations A7 and A9 in Wheeler et al. (2005; note error in the  $F_W$  term of their Equation A9: it should be  $F_W/(1 - F_W)$ ).

#### Error propagation

We used standard procedures (Bernard and Epp 1995) to propagate standard errors from parameters whose variation was directly determined from individual stem measurements (e.g.,  $R_{Xa}$ , vessel density,  $R_C$ ,  $R_L$ ,  $R_W$ ,  $L$ ,  $D$ ,  $F$ , length fraction, pit-field fraction and contact fraction) to parameters calculated from species means where errors had to be combined ( $A_p$ ,  $A_v$ ,  $F_p$ ,  $F_L$ ,  $r_p$  and  $r_w$ ). For the seven species where the stem shortening method was used, the standard error of  $R_{Xa}$  was estimated from the regression of  $R_{Xa}$  versus percentage of open vessels for pooled data of all stems per species.

## Results

#### Vulnerability curves and the safety versus efficiency relationship

Two types of vulnerability curves were observed (Figure 1). The six ring-porous species and the vine, *P. montana*, tended to have relatively high maximum  $K_{Xa}$  for non-embolized xylem ( $K_{Xa-max}$ ), but an abrupt decline in  $K_{Xa}$  with pressure (Figure 1, *Q. prinus* and *M. alba* curves). The seven diffuse-porous species (and diffuse-porous species from Wheeler et al. 2005) tended to have a lower  $K_{Xa-max}$  but generally retained  $K_{Xa}$  more effectively with pressure (Figure 1, *Acer grandidentatum*, *Acer negundo* and *C. crassifolius* curves; *A. negundo* data from Sperry et al. 2005). The abrupt drop in  $K_{Xa}$  observed in the ring-porous type of curve was not an artifact of the centrifuge method, because the same pattern was seen in the curves

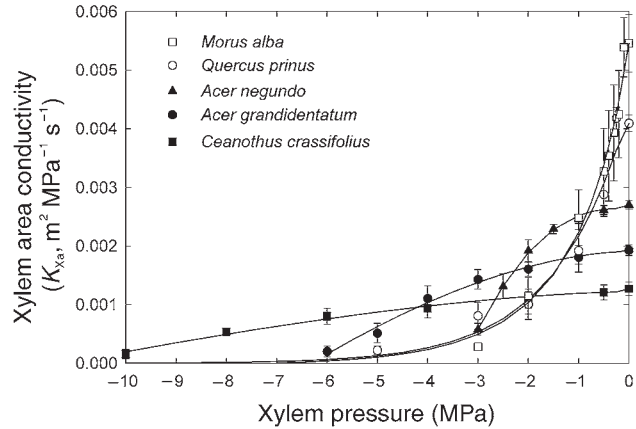


Figure 1. Vulnerability curves for selected species showing the decline in xylem conductivity per sapwood area ( $K_{Xa}$ ) with negative xylem pressure. Open symbols ( $\square$  and  $\circ$ ) are ring-porous species and solid symbols ( $\blacktriangle$ ,  $\bullet$  and  $\blacksquare$ ) are diffuse-porous species. Values are means  $\pm$  SE,  $n = 6$  stems per species.

obtained by the air-injection method (Figure 2). The two methods were statistically identical at all pressures in the two *Quercus* species and at three of five pressures in *R. trilobata*. In the latter species, the centrifuge method tended to produce greater loss of conductivity for the same pressure than the air-injection method, but the shape of the curve was similar, with an abrupt conductivity loss at modest pressure. Although the stems for the centrifuge method were shorter (14.2 cm) than for the air-injection method (22 cm minimum) and had a greater portion of open vessels running through the stem (e.g., 15 versus 5.4% in *Q. gambelii* and 3 versus 0.4% in *R. trilobata* based on vessel length distributions), this did not appear to influence the curves. The data for species in Figure 2 were obtained from different populations, stem ages and season than for the main survey.

In the vine *P. montana*, the curves obtained by the centrifuge method were quite variable and generally showed greater vulnerability than those obtained by the air-injection method, although the basic curve shape was similar (data not shown). The variability was attributed to the extremely long and wide vessels in this vine, 35% of which were estimated to run through the 14.2 cm segments required for the centrifuge method. Open vessels may not have been the problem, but rather the problem may have been that the vessels were so wide (mean  $D = 150 \mu\text{m}$ ) that they emptied by gravity if the stem segment was tilted to the vertical. To avoid the difficulty of handling this material (the centrifuge method requires moving and manipulating the stem multiple times), we used the air-injection curve for this species. For all other species the centrifuge method was used.

For the species in Figure 1, the higher the  $K_{Xa-max}$  (the y intercept), the steeper the loss of conductivity at modest pressure (the slope) and, in general, the lower the pressure required to eliminate conductivity (the x intercept). This is consistent with a trade-off between safety and conducting efficiency: for a given pressure, there is a limited range of vulnerability curves

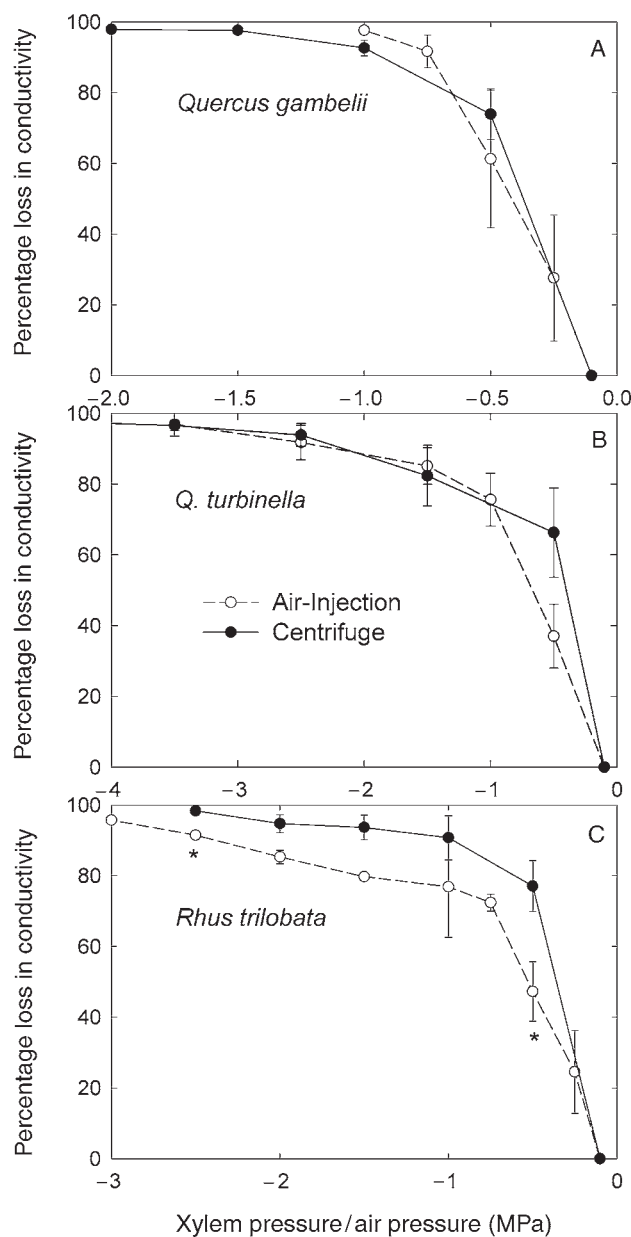


Figure 2. Vulnerability curves of three ring-porous species showing percentage loss of conductivity versus pressure. The curves compare the centrifuge (●) and air-injection (○) methods for each species. Asterisks indicate significantly different means. Values are means  $\pm$  SE for  $n = 3$  (air-injection) and  $n = 10$  (centrifuge) methods. The methods comparison for *Q. gambelii* was from a different population and time of year than the data for the anatomy–vulnerability survey.

that provide optimal (maximum)  $K_{Xa}$ . Notably, this optimal curve can be associated with a very high native embolism. For example, at a pressure of  $-0.8$  MPa, the “best” vulnerability curve with the highest  $K_{Xa}$  at  $-0.8$  MPa is for *M. alba*, although at this pressure, this species would be about 50% embolized. In contrast, the three diffuse-porous species at  $-0.8$  MPa would be less than 10% embolized, yet still have a lower  $K_{Xa}$  because their  $K_{Xa-max}$  (intercept) values were so much lower. This pattern is maintained at lower pressures. For example, at  $-3$  MPa,

the best curve is for *A. grandidentatum* despite its being about 35% embolized at this pressure. *Ceanothus crassifolius* at  $-3$  MPa is hardly embolized at all, yet has the lower  $K_{Xa}$ .

#### Scaling of safety versus efficiency parameters across species

Representing the slope of the vulnerability curve by the mean cavitation pressure, a safety versus efficiency relationship was evident across all 29 species (including the 15 from Wheeler et al. 2005, Table 2) with more negative mean cavitation pressure corresponding to higher xylem area resistivity ( $R_{Xa} = 1/K_{Xa-max}$ ; Figure 3A). Thus, the trend seen in Figure 1 extends across all species in the data set. The two vine species with some of the widest and longest vessels (Pum, Vv; Figure 4) had the lowest  $R_{Xa}$  and among the least negative cavitation pressure (Figure 3A). The ring-porous species had similar or even higher  $R_{Xa}$  for the same cavitation pressure as the diffuse-porous species (Figure 3A, asterisk symbols, dashed line), despite their tendency to have wider and longer vessels (Figure 4, dashed lines). The ring-porous species also tended to cluster towards the vulnerable end of the cavitation pressure range (Figure 3A).

The  $R_{Xa}$  is a function of the  $R_{Ca}$  and the total cross-sectional area of the xylem occupied by vessels:  $R_{Xa} = R_{Ca} \times \text{xylem/vessel area ratio}$ . The  $R_{Ca}$  also increased with cavitation pressure (Figure 3B,  $r^2 = 0.60$  for all species), but more weakly than the  $R_{Xa}$  scaling (Figure 3A,  $r^2$  for all species = 0.86). This was because ring-porous species had lower  $R_{Ca}$  for the same pressure than the other species (Figure 3B, dashed line), consistent with their tendency to have larger vessels at the same pressure (Figure 4, dashed lines). Despite their lower  $R_{Ca}$ , the ring-porous species did not have a reduced  $R_{Xa}$  because their xylem/vessel area ratio was much higher for the same pressure than other species (Figure 3C, dashed line). The low vessel area in ring-porous species cancelled out the effect of their lower  $R_{Ca}$  at the tissue level, yielding comparable or higher  $R_{Xa}$  as diffuse-porous species.

All species considered, the efficiency versus safety trade-off at the sapwood  $R_{Xa}$  level was much more severe than at the conduit  $R_{Ca}$  level. The  $R_{Xa}$  increased 13-fold from a cavitation pressure of  $-0.58$  to  $-8.1$  MPa, versus a 4.5-fold increase in  $R_{Ca}$ . The steeper increase in  $R_{Xa}$  was owed to a strong increase in the xylem/vessel area ratio with cavitation pressure (Figure 3C). This in turn resulted from a decrease in vessel diameter with more negative cavitation pressure (Figure 4,  $r^2 = 0.71$ ), which was more important than a weak tendency for vessel density to increase ( $r^2 = 0.25$ ; data not shown).

The increase in  $R_{Ca}$  with safety was nearly equally divided between the  $R_L$  and  $R_W$  components (Figure 5). On average, 56% of the vessel resistivity was in the end-walls and 44% in the lumen. Mean  $F = R_L/R_W$  was  $0.85 \pm 0.078$ . This ratio did not differ between ring-porous and diffuse-porous species measured for this paper, or between the Wheeler et al. (2005) data and the species added in this study.

In contradiction to the pit resistance hypothesis modeled previously (Figure 6, circles; Sperry and Hacke 2004), the pooled data set showed no increase in  $r_p$  with more negative

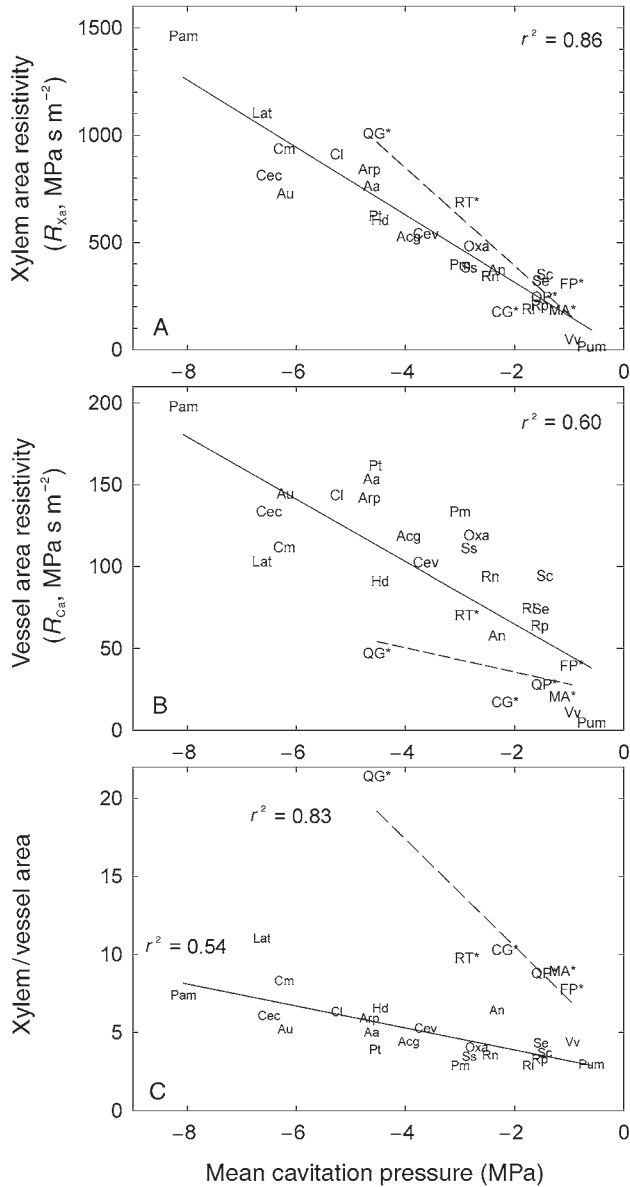


Figure 3. Safety versus efficiency trade-off across the 29-species data set. Species symbols are given in Tables 1 and 2. Dashed line and asterisked double-capital symbols identify ring-porous species. For clarity, error bars on species means are not shown. (A) Xylem area resistivity ( $R_{Xa}$ ) versus mean cavitation pressure. Solid line is regression through complete data set. Standard error averaged 7% of  $R_{Xa}$ . (B) Vessel area resistivity ( $R_{Ca}$ ) versus mean cavitation pressure. Solid line is regression for complete data set. Standard error averaged 13% of  $R_{Ca}$ . (C) Xylem/vessel cross-sectional area ratio. Dashed line is regression for ring-porous species, solid line is separate regression for diffuse-porous species and vines. Standard error averaged 9% of means.

cavitation pressure (Figure 6, species symbols). Instead, there was a weakly significant ( $r^2 = 0.17$ ) opposite trend. Measured  $r_p$  was also substantially greater than modeled (Figure 6). The 29-species data set showed large variation in  $r_p$ , but it was unrelated to safety from cavitation or to functional group (ring-porous versus diffuse-porous). The estimated standard

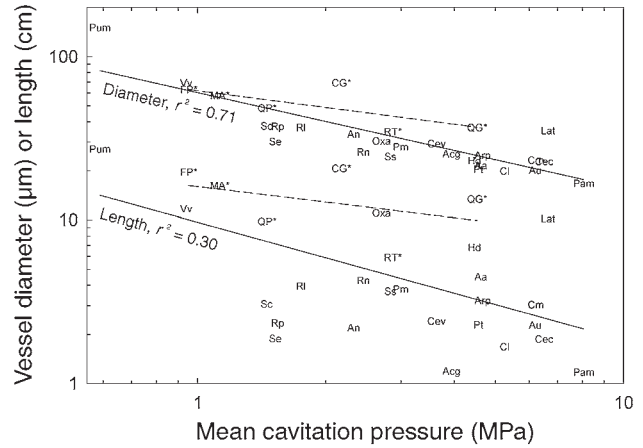


Figure 4. Scaling of vessel diameter ( $D$ ) and length ( $L$ ) with mean cavitation pressure (shown as absolute value for log scaling). Dashed lines and asterisked double-capital symbols identify ring-porous species. Standard error averaged 12% of mean  $L$  and 6% of mean  $D$ . Species symbols are given in Tables 1 and 2.

error averaged 33% of  $r_p$ . This high percentage was a result of the propagation of error through multiple calculations.

In confirmation of the pit area hypothesis, the addition of data for 14 species of diverse vessel size and safety reinforced the strong inverse relationship between total  $A_p$  and mean cavitation pressure across all species with no clear distinction between ring- and diffuse-porous types (Figure 7A,  $r^2 = 0.77$ ). Total vessel surface area ( $A_v$ ) also scaled with increasing mean cavitation pressure, though much more weakly (Figure 7A,  $r^2 = 0.47$ ) because of variation in the fraction of vessel surface that was pitted (the pit fraction,  $F_p = A_p/A_v$ , Figure 7B). For example, the ring-porous species tended to have higher  $A_v$  for the same cavitation pressure than diffuse-porous species (Figure 7A, asterisked symbols, dashed line) because the ring-porous  $F_p$  tended to be low for the same pressure compared with  $F_p$  of many diffuse-porous species (Figure 7B, dashed line).

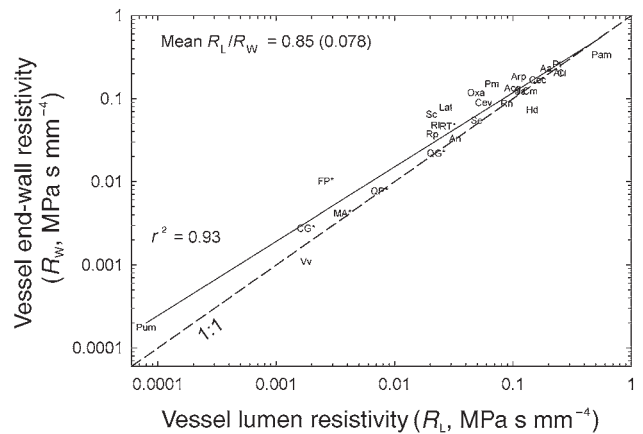


Figure 5. Scaling of vessel end-wall resistivity ( $R_W$ ) with vessel lumen resistivity ( $R_L$ ). Dashed line is 1:1. Mean  $R_L/R_W = F$  ratio was  $0.85 \pm 0.078$ . Standard error averaged 13% of mean  $R_L$  and 19% of mean  $R_W$ . Species symbols are given in Tables 1 and 2.

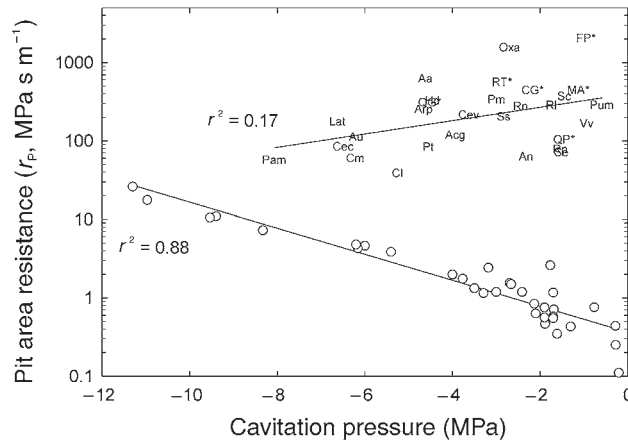


Figure 6. Pit area resistance ( $r_p$ ) versus cavitation pressure. Modeled values from Sperry and Hacke (2004) shown as open circles. Standard error averaged 33% of the mean for measured values. Species symbols are given in Tables 1 and 2.

The  $F_p$  averaged  $6.3 \pm 0.9\%$  (range: 0.4–21%) across the full data set. Whereas the Rosaceae-dominated data set of Wheeler et al. (2005) showed a significant drop in  $F_p$  with mean cavitation pressure, addition of another 14 species eliminated this trend. In the full data set,  $F_p$  did not vary significantly with safety from cavitation (Figure 7B). The variation in  $F_p$  was primarily in the contact fraction rather than the pit-field fraction (Table 1).

The  $A_p$ , besides being hypothetically responsible for setting cavitation pressure, was also the dominant influence on the variation in  $R_{Ca}$  compared with the other parameters in the summary Equation 5 (Figure 8). The  $R_{Ca}$  changed 165-fold for the observed 593-fold range in  $A_p$  (Figure 8,  $A_p$  curve). The next most important determinants of  $R_{Ca}$  were  $r_p$  and  $F_p$ , causing only a 5-fold change in  $R_{Ca}$  for their 53-fold variation (Figure 8,  $r_p$  and  $F_p$  curves).

The  $F = R_L/R_W$  fraction had a limited range ( $0.85 \pm 0.078$ , range 0.26–1.98; Figure 5) and a comparatively minor 1.4-fold effect on  $R_{Ca}$  across its range (Figure 8, solid  $F$  curve). As Equation 5 indicates, there is an optimal  $F$  that minimizes  $R_{Ca}$  which is emphasized graphically by the short-dashed extension of the  $F$  curve in Figure 8. The observed  $F$  range kept  $R_{Ca}$  near this optimum. The  $F_L = L'/L$  fraction varied little in the data set (Table 1) and had a trivial 1.1-fold influence on  $R_{Ca}$  (data not shown).

Overall, the variation in  $A_p$  explained 72% of the variation in  $R_{Ca}$  (data not shown). Because  $A_p$  is also linked to cavitation pressure (Figure 7A), it provides a basis for the safety versus efficiency trade-off (Figures 1 and 3): low  $A_p$  may be required for more negative cavitation pressure, and it also results in greater xylem resistivity. The effect of  $A_p$  on resistivity was through its link to vessel surface area,  $A_v$  (Figure 7A), which resulted from the limited range of  $F_p$  (Figure 7B). The  $A_v$  in turn was related to vessel  $D$  and  $L$  and their respective declines with increasingly negative cavitation pressure (Figure 4).

As Equation 6 indicates,  $L$  versus  $D$  scaling is a complex function of several variables. However, because the terms be-

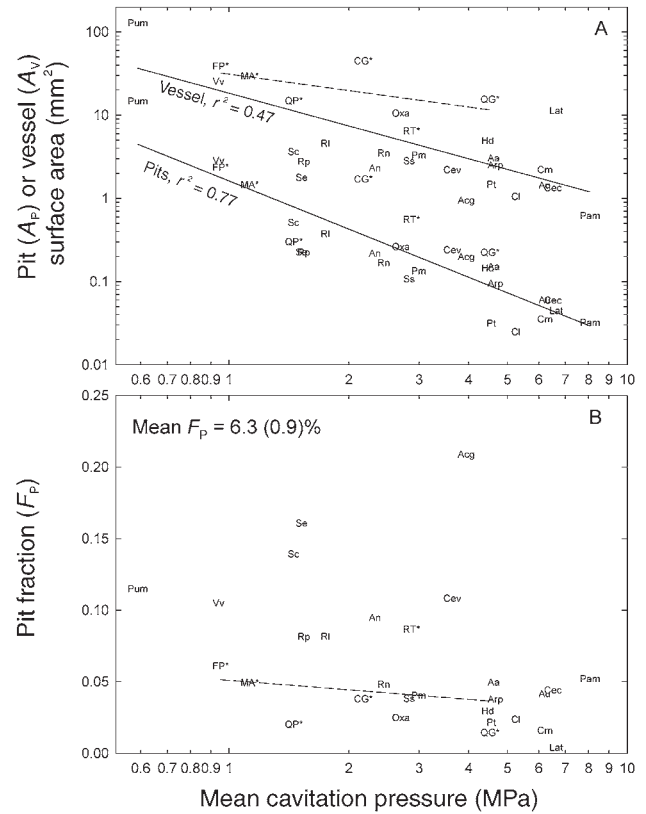


Figure 7. (A) Pit membrane ( $A_p$ ) and vessel ( $A_v$ ) surface areas versus mean cavitation pressure (shown as absolute value for log-scaling). Dashed line highlights ring-porous species in  $A_v$  plot. Standard error averaged 19% of  $A_p$  and 14% of  $A_v$ . (B) Pit fraction ( $F_p = A_p/A_v$ ) versus mean cavitation pressure. Mean  $F_p$  was  $6.3 \pm 0.9\%$ . Dashed line highlights ring-porous species. Standard error averaged 13% of mean. Species symbols are given in Tables 1 and 2.

sides  $D$  in Equation 6 ( $F$ ,  $r_p$ ,  $F_L$  and  $F_p$ ) did not vary systematically with  $D$ ,  $L$  scaled with  $D$  to the  $3/2$  power across the wide range of lengths and diameters in the data set (Figure 9,  $r^2 = 0.63$ ).

**Discussion**

We obtained evidence for a significant safety versus efficiency trade-off in xylem hydraulic function (Figures 1 and 3). This trade-off, together with a requirement for greater construction cost in cavitation-resistant xylem (Hacke et al. 2001a), may explain why angiosperm xylem is usually not more resistant than required by the normal negative pressure range a species experiences. The data reinforced the pit area hypothesis while contradicting the pit resistance hypothesis as an explanation for this trade-off. Increasing safety from cavitation was strongly associated with decreasing pit area per vessel (Figure 7A,  $r^2 = 0.77$ ), but not with increasing pit area resistance (Figure 6). Mean pit membrane porosity apparently does not correlate with cavitation pressure as previously modeled (Sperry and Hacke 2004). If air-seeding occurs at the largest membrane pore per vessel, this limiting pore may be quite

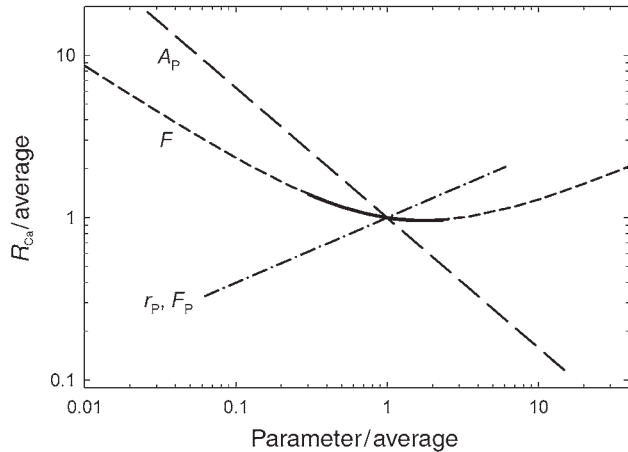


Figure 8. Sensitivity of vessel area resistivity ( $R_{Ca}$ ) to changes in Equation 5 variables ( $A_p$ ,  $F$ ,  $r_p$  and  $F_p$ ) relative to their mean values. Variable  $F_L$  in Equation 5 is not shown because it has minimal importance. Each parameter curve shows the  $R_{Ca}$  calculated from Equation 5 for the full range of that parameter with the other variables constant at their mean values. The dotted curve for  $F$  extends beyond the actual  $F$  range in the data set (solid portion of curve) to emphasize that there is an optimal  $F$  that minimizes  $R_{Ca}$ . Abbreviations:  $A_p$  = total inter-vessel pit membrane surface area of vessel;  $F$  = lumen to end-wall resistivity ratio;  $r_p$  = pit membrane area resistance;  $F_p$  = pit fraction; and  $F_L$  = length between vessel end-wall to vessel length ratio.

rare. Some support for this comes from observations of pit membranes where most of the membrane pores are too small to observe, and pores of air-seeding size are relatively few and far-between (Sperry and Tyree 1988, Sano 2004).

The pit area hypothesis explains the observed safety versus efficiency trade-off (Figure 3) as follows. To achieve a given safety from cavitation, the pit area per vessel must be limited, because this limits the mean size of the largest membrane pore

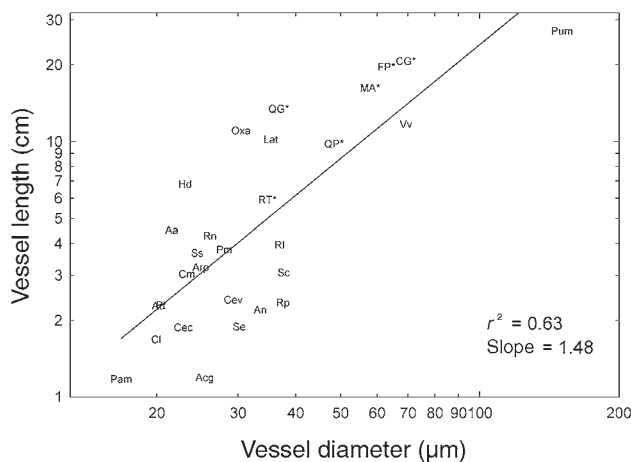


Figure 9. Scaling of vessel length ( $L$ ) with diameter ( $D$ ). Slope of the log-log plot was 1.48 as indicated from Equation 6 when the other equation parameters do not vary with  $D$ . Species symbols are given in Tables 1 and 2.

per vessel and hence its susceptibility to air-seeding. A limited pit area also limits the vessel surface area (Figure 7A) which translates into a limit on vessel diameter and length (Figure 4) and hence its resistivity (Figure 3B).

In theory, it is not necessary for pit area to limit vessel surface area if the fraction of the vessel wall that is pitted (the pit fraction,  $F_p$ ) can become infinitely small. If that were possible, a small pit area for safety could reside in a large and wide vessel for efficiency. Accordingly, a corollary of the pit area hypothesis is that  $F_p$  should be small. This was generally the case, with a mean  $F_p$  of  $6.3 \pm 0.9\%$  (Figure 7B), with four species below 2% (Figure 7B). However, none were below the 0.4% extreme for *L. tridentata*. In the Rosaceae-dominated data set of Wheeler et al. (2005), there was a significant decrease in  $F_p$  with safety from cavitation, which would help to minimize the loss of conducting efficiency. However, this seemingly adaptive trend was not supported by the inclusion of more diverse species. One important disadvantage of a low pit fraction is a more rigidly axial flow path with less ability for water to flow laterally to circumvent wounds or to provide flexibility in distribution of resources from root to crown sections (Oriens et al. 2004).

Variation in the safety versus efficiency trade-off at the xylem tissue level (Figure 3A) resulted from a variety of sources, beginning with variation in the proposed cause-and-effect relationship between pit area per vessel and the cavitation pressure (Figure 7A). Although this relationship was strong ( $r^2 = 0.77$ ), there was still considerable variation that may be more than just measurement error. Among species, those with more pit area per vessel for the same maximum pore size (e.g., CG, QG in Figure 7A) have the potential to be more efficient with the same safety from cavitation. There was also variation in other aspects of vessel structure that may not be causally linked to cavitation safety, of which  $r_p$  and  $F_p$  were most consequential for resistivity at the vessel level (Figure 8). Scaling to the tissue level, the variation in the xylem/vessel area ratio (Figure 3C) creates further flexibility in the  $R_{Xa}$  versus safety relationship. With all of these intermediate steps between safety and efficiency, it follows that the trade-off will be statistically noisy and nonexistent in more limited data sets (Hacke and Sperry 2001, Jacobsen et al. 2005).

Our  $r_p$  estimates showed tremendous variation, from 39 to 2040 MPa s m<sup>-1</sup> (Figure 6). Doubtless, some of this variation resulted from the imprecise and indirect method used to estimate  $r_p$ , with standard errors averaging 33% of the mean value. Pit resistances of this magnitude should be over 99% determined by the pit membrane (versus aperture resistance), corresponding to a prevailing membrane pore diameter between 3 and 8 nm (Wheeler et al. 2005). This pore size is similar to the average size range estimated experimentally in some plants (Shane et al. 2000, Choat et al. 2003, 2004) lending some credence to our estimates, although similar experiments on two chaparral species found larger pore sizes (Jarbeau et al. 1995).

#### Scaling of vessel resistivities and dimensions

The relatively tight scaling between  $R_L$  and  $R_W$  components of

vessel resistivity (Figure 5) maintained a narrow range of  $R_L/R_W = F$  ( $0.85 \pm 0.078$ ) across four orders of resistivity magnitude. This  $F$  ratio corresponded with an average of 56% of the vessel resistivity residing in the end-wall. According to Equation 5, the possible significance of this restricted  $F$  range was that it maintained  $R_{Ca}$  close to its minimum for a vessel where other variables ( $A_p$ ,  $F_p$ ,  $F_L$  and  $r_p$ ) are constant (Figure 8). Based on the pit area hypothesis,  $A_p$  is constrained for a given cavitation pressure and  $F_p$  should be low and thus have limited variability as observed (Figure 7B, mean  $F_p = 6.3 \pm 0.9\%$ ). Empirically,  $F_L$  differed little across the data set (Table 1). The  $r_p$ , though quite variable (Figure 6), was independent of pit area. Thus, the restricted  $F$  range is consistent with optimizing vessel resistivity under the constraints of the pit area hypothesis.

This scaling of  $R_W$  with  $R_L$  (Figure 5) is consistent with an underlying scaling of  $D$  and  $L$  (Figure 9). Across species, wide vessels tended to be long, whereas narrow vessels tended to be short, as observed in many other studies. Vessels in ring-porous trees and vines can be both wider and longer than their counterparts in diffuse-porous wood (Zimmermann and Jeje 1981, Sperry et al. 1994) and vessels in stems are narrower and shorter than in roots (Zimmermann and Potter 1982). In a survey of lianas, narrow vessels were almost always short, whereas wide vessels ranged from short to long (Ewers and Fisher 1989). Fisher et al. (2002) found a weak correlation between maximum vessel length and maximum diameter in rattans.

According to Equation 6 and as shown in Figure 9,  $L$  increases with  $D^{3/2}$  when  $F$  and the other parameters in Equation 5 ( $r_p$ ,  $F_p$  and  $F_L$ ) do not vary systematically with vessel size (Lancashire and Ennos 2002). The variation in  $r_p$  and  $F_p$  across the data set make the  $L$  versus  $D$  relationship quite noisy, and the  $3/2$  scaling is evident only across the wide range of vessel sizes in our data set. The relationship is heavily influenced by the large vessels of *P. montana* (Figure 9, Pum) and it remains to be seen whether the  $3/2$  scaling will be confirmed when a greater variety of big-vessel species are analyzed. Wheeler et al. (2005) found no relationship between  $D$  and  $L$ , probably because of the lack of more big-vessel species in that restricted data set.

#### *Implications of ring-porous, diffuse-porous and vine wood anatomies*

A consequence of a trade-off between vessel size and vulnerability is that it can be advantageous for a species to operate at very high native embolism levels as discussed in relation to the vulnerability curves in Figure 1. If the vulnerability curves shown in Figure 1 are plotted in the standard way, as a percentage loss in maximum conductivity versus pressure (e.g., as in Figure 2), the curves we observed for ring-porous trees and vines seem tremendously non-adaptive: showing big losses of relative conductivity at normal operating pressures compared with curves from diffuse-porous species where the native conductivity loss is negligible. Nevertheless, the curves appear to be valid based on the agreement between centrifuge and air-in-

jection methods (Figure 2). Tibbetts and Ewers (2000) found similar vulnerability curves in two lianas when using the bench-top dehydration method. Only when such curves are plotted in absolute conductivities, as in Figure 1, does their adaptive value become apparent—even though they may have a high percentage loss of conductivity at their native pressures, the ring-porous type of curve can still be compatible with a higher (or equal) conductivity than that of plants showing no loss of conductivity at the same pressure. An important detail is that the shape of the vulnerability curve depends on whether the curve is obtained from flushed stems where native embolism has been reversed (e.g., as in Figure 2) or whether it is determined from non-flushed stems. In the latter case (e.g., *Q. gambelii* curve from Sperry and Sullivan 1992), there will be little or no drop in conductivity until pressures fall below the minimum experienced by the stems in the field.

The curves we found in vines and ring-porous trees exemplify a sacrificial strategy of growing big and efficient vessels, many of which will lose function at normal operating pressure, but those remaining are still more efficient than smaller and inherently safer vessels. This strategy is illustrated in Figure 10A. The theoretical curves were generated with a Weibull function (Equation 1) by linking the Weibull  $b$  parameter (pressure at 63% loss of conductivity) to the  $K_{Xa-max}$  parameter as dictated by the scaling relationships between  $A_p$  and pressure (Figure 7A) and using mean values for all other parameters in Equation 5. The Weibull  $c$  parameter was held constant. These curves assume that the xylem/vessel area ratio is constant at the mean of 6.5 for the data set. For a single  $x$ -axis xylem pressure, there is a single optimal curve: at  $-1.1$  MPa this is Curve 5, at  $-1.3$  MPa it is Curve 4, at  $-1.5$  MPa it is Curve 3, and at  $-2.0$  MPa it is Curve 2. At each pressure, the native embolism corresponding to the optimal curve is about 50%.

The disadvantage of the sacrificial strategy is obvious for the more vulnerable curves: a slight drop in pressure from its optimal value causes a severe drop in conductivity. For example, Curve 5 is optimal for  $-1.1$  MPa, but quite sub-optimal for  $-1.5$  MPa. This sensitivity to pressure variation is most severe at modest negative pressures. The sacrificial strategy may be adaptive for a habitat or growth form where water stress is generally modest. This strategy seems less beneficial when frequent periods of severe water stress require conductivity to be sustained over a broad range of pressures.

One way to mitigate the trade-off between vessel size and vulnerability illustrated in Figure 10A is to have small vessels for safety, but to minimize the xylem/vessel area ratio by packing the maximum number of small vessels in the xylem. This vessel packing strategy is shown in Figure 10B. Here, each curve has the same Weibull  $b$  and  $c$  parameters (from curve 3 in Figure 10A) and thus the same individual vessel conductivity per vessel area. However, the xylem/vessel area ratio is changed as indicated below the  $K_{Xa-max}$  intercept of each curve. The mean ratio was 6.5 (Figure 10B, central 6.5 curve). Decreasing this ratio to 3 more than doubles the  $K_{Xa-max}$  without making the xylem more vulnerable to cavitation (Figure 10B, top 3 curve). Increasing the area ratio to 28 has the

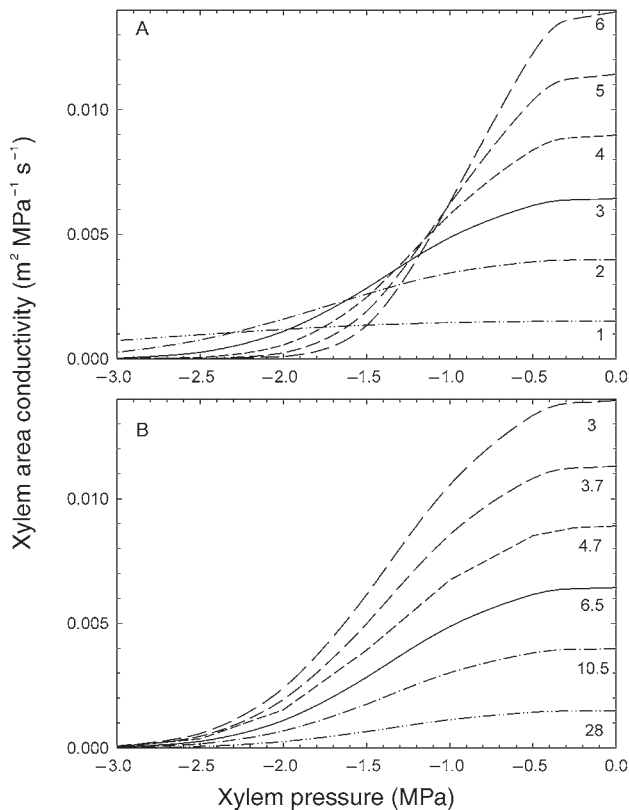


Figure 10. Two mechanisms for coping with a safety versus efficiency trade-off as illustrated with theoretical vulnerability curves. Curves were calculated from the Weibull function (Equation 1) using  $c = 2.7$  and linking  $b$  to vessel pit area ( $A_p$ ) via the observed scaling in Figure 7A. The vessel cross-sectional area resistivity ( $R_{Ca}$ ) was calculated from  $A_p$  by Equation 5 with mean values for the other variables ( $F$ ,  $r_p$ ,  $F_p$  and  $F_L$ ). The maximum xylem conductivity for non-embolized xylem ( $K_{Xa-max}$ ) was calculated from  $R_{Ca}$  and the xylem/vessel area ratio. (A) The sacrificial strategy. All curves have the same xylem/vessel area ratio (= 6.5 data average) and differ only in their Weibull  $b$  parameter and corresponding  $K_{Xa-max}$ . Greater  $K_{Xa-max}$  corresponds with more vulnerable xylem (smaller  $b$ ) according to the pit area hypothesis. It is advantageous to have vulnerable xylem and sacrifice approximately 50% of the  $K_{Xa-max}$  because the residual conductivity can be higher than that of xylem with more cavitation-resistant curves which necessarily starts out at a lower  $K_{Xa-max}$ . (B) The vessel-packing strategy. All curves have the same Weibull  $b$  parameter and vessel pit area (matching Curve 3 in A) and differ only in the xylem/vessel area ratio (number on curves). Decreasing this ratio by packing more vessel area into the xylem increases  $K_{Xa-max}$  without sacrificing the vulnerability of individual vessels to cavitation. Abbreviations:  $F$  = lumen to end-wall resistivity ratio;  $r_p$  = pit membrane area resistance;  $F_p$  = pit fraction; and  $F_L$  = length between vessel end-wall to vessel length ratio.

opposite effect, reducing the  $K_{Xa-max}$  by more than 4-fold (Figure 10B, lower 28 curve). The vessel packing strategy can provide high  $K_{Xa-max}$  and stable  $K_{Xa}$  over a potentially broad pressure range by minimizing the xylem/vessel area ratio.

Both the sacrificial and vessel packing strategies combine to influence the real vulnerability curves in Figure 1. The ring-porous species in our study exploited the sacrificial strategy by having relatively high xylem/vessel area ratios (Figure 3C,

mean = 11.1) and relatively large, vulnerable vessels with high conductivities (= low  $R_{Ca}$ , Figure 3B). The diffuse-porous species we sampled exploited the packing strategy with lower xylem/vessel area ratios (Figure 3C, mean = 5.1) and achieved similarly high  $K_{Xa-max}$  (=  $1/R_{Xa}$ ) as ring-porous species with the same mean cavitation pressure (Figure 3A).

There may be limits to the packing strategy. The xylem/vessel area ratio cannot drop below 1, and in practice it does not approach this minimum (observed data set minimum = 2.9, Figure 3C). Presumably this is because there are space requirements for ray and axial parenchyma cells and also mechanical limitations to reducing the fiber area in angiosperm xylem. The relatively high xylem/vessel area ratios for ring-porous trees (mean 11.1) versus diffuse-porous trees (mean 5.1) may reflect mechanical vulnerability of larger vessels in free-standing stems. Vines, not being self-supporting and free of this possible mechanical constraint, can have vessels as large or larger than those of ring-porous trees while having low xylem/vessel area ratios comparable to those of diffuse-porous trees (Figures 3C and 4). Vines can exploit both the sacrificial and vessel packing strategy, and achieve the lowest  $R_{Xa}$  of all the species in the entire data set (Figure 3A, Vv, Pum data points).

Additional evidence for a mechanical limit on the packing strategy is the increase in xylem/vessel area ratio with increasing safety from cavitation (Figure 3C). The increase in this ratio costs the plant by amplifying the safety versus efficiency trade-off at the single vessel level—resulting in a much steeper trade-off between cavitation pressure and  $R_{Xa}$  than for  $R_{Ca}$  (cf. Figures 3A and 3B). The mechanical stress imposed by increasingly negative sap pressures in cavitation-resistant xylem correlates with increasing wood density in angiosperms (Hacke et al. 2001a) and an increasing fiber fraction and density (Jacobsen et al. 2005). Perhaps a dense and extensive fiber matrix is required to compensate for these pressure-derived stresses (Hacke and Sperry 2001). More information is needed on the importance of wood anatomy for bearing mechanical stresses associated with negative xylem pressure in combination with structural support of canopies.

#### Acknowledgments

We thank Stephen Davis for collecting and shipping us material of *Ceanothus crassifolius*. Financial support was provided from NSF-IBN-0416297. The second author's mother (Jo Sperry) generously assisted in collection and shipping of species from North Carolina.

#### References

- Alder, N.N., W.T. Pockman, J.S. Sperry and S. Nuismer. 1997. Use of centrifugal force in the study of xylem cavitation. *J. Exp. Bot.* 48:665–674.
- Bernard, C. and C. Epp. 1995. Laboratory experiments in college physics. John Wiley & Sons, New York. 387 p.
- Carlquist, S. 1988. Comparative wood anatomy. Springer-Verlag, Berlin, 436 p.
- Choat, B., M. Ball, J. Lully and J. Holtum. 2003. Pit membrane porosity and water stress-induced cavitation in four co-existing dry rain forest tree species. *Plant Physiol.* 131:41–8.

- Choat, B., S. Jansen, M.A. Zwieniecki, E. Smets and N.M. Holbrook. 2004. Changes in pit membrane porosity due to deflection and stretching: the role of vested pits. *J. Exp. Bot.* 55:1569–1575.
- Choat, B., E.C. Lahr, P.J. Melcher, M.A. Zwieniecki and N.M. Holbrook. 2005. The spatial pattern of air-seeding thresholds in mature sugar maple trees. *Plant Cell Environ.* 28:1082–1089.
- Cochard, H., P. Cruiziat and M.T. Tyree. 1992. Use of positive pressures to establish vulnerability curves: Further support for the air-seeding hypothesis and implications for pressure-volume analysis. *Plant Physiol.* 100:205–209.
- Crombie, D.S., M.F. Hipkins and J.A. Milburn. 1985. Gas penetration of pit membranes in the xylem of *Rhododendron* and other species. *Planta* 163:27–33.
- Ewers, F.W. and J.B. Fisher. 1989. Variation in vessel length and diameter in stems of six tropical and subtropical lianas. *Am. J. Bot.* 76:1452–1459.
- Fisher, J.B., H.T.W. Tan and L.P.L. Toh. 2002. Xylem of rattans: vessel dimensions in climbing palms. *Am. J. Bot.* 89:196–202.
- Hacke, U.G. and J.S. Sperry. 2001. Functional and ecological xylem anatomy. *Perspect. Plant Ecol.* 4:97–115.
- Hacke, U.G., J.S. Sperry, B.E. Ewers, D.S. Ellsworth, K.V.R. Schäfer and R. Oren. 2000. Influence of soil porosity on water use in *Pinus taeda*. *Oecologia* 124:495–505.
- Hacke, U.G., J.S. Sperry and J. Pittermann. 2004. Analysis of circular bordered pit function. II. Gymnosperm tracheids with torus-margo pit membranes. *Am. J. Bot.* 91:386–400.
- Hacke, U.G., J.S. Sperry, W.P. Pockman, S.D. Davis and K.A. McCulloh. 2001a. Trends in wood density and structure are linked to prevention of xylem implosion by negative pressure. *Oecologia* 126:457–461.
- Hacke, U.G., V. Stiller, J.S. Sperry, J. Pittermann and K.A. McCulloh. 2001b. Cavitation fatigue: embolism and refilling cycles can weaken cavitation resistance of xylem. *Plant Physiol.* 125:779–786.
- Hargrave, K.R., K.J. Kolb, F.W. Ewers and S.D. Davis. 1994. Conduit diameter and drought-induced embolism in *Salvia mellifera* Greene (Labiatae). *New Phytol.* 126:695–705.
- Hubbard, R.M., V. Stiller, M.G. Ryan and J.S. Sperry. 2001. Stomatal conductance and photosynthesis vary linearly with plant hydraulic conductance in ponderosa pine. *Plant Cell Environ.* 24:113–121.
- Jacobsen, A.L., F.W. Ewers, R.B. Pratt, W.A. Paddock and S.D. Davis. 2005. Do xylem fibers affect vessel cavitation resistance? *Plant Physiol.* 139:546–556.
- Jarbeau, J.A., F.W. Ewers and S.D. Davis. 1995. The mechanism of water-stress-induced embolism in two species of chaparral shrubs. *Plant Cell Environ.* 18:189–196.
- Lancashire, J.R. and A.R. Ennos. 2002. Modeling the hydrodynamic resistance of bordered pits. *J. Exp. Bot.* 53:1485–1493.
- Linton, M.J., J.S. Sperry and D.G. Williams. 1998. Limits to water transport in *Juniperus osteosperma* and *Pinus edulis*: implications for drought tolerance and regulation of transpiration. *Func. Ecol.* 12:906–911.
- Martinez-Vilalta, J., E. Prat, I. Oliveras and J. Pinol. 2002. Xylem hydraulic properties of roots and stems of nine Mediterranean woody species. *Oecologia* 133:19–29.
- Meinzer, F.C. and D.A. Grantz. 1990. Stomatal and hydraulic conductance in growing sugarcane: Stomatal adjustment to water transport capacity. *Plant Cell Environ.* 13:383–388.
- Orians, C., M. van Vuuren, N. Harris, B. Babst and G. Ellmore. 2004. Differential sectoriality in long-distance transport in temperate tree species: evidence from dye flow, <sup>15</sup>N transport, and vessel element pitting. *Trees* 18:501–509.
- Pockman, W.T. and J.S. Sperry. 2000. Vulnerability to xylem cavitation and the distribution of Sonoran Desert vegetation. *Am. J. Bot.* 87:1287–1299.
- Sano, Y. 2004. Intervascular pitting across the annual ring boundary in *Betula platyphylla* var. *japonica* and *Fraxinus mandshurica* var. *japonica*. *IAWA J.* 25:129–140.
- Shane, M.W., M.E. McCully and M.J. Canny. 2000. Architecture of branch-root junctions in maize: structure of the connecting xylem and the porosity of pit membranes. *Ann. Bot.* 85:613–624.
- Sperry, J.S. and M.T. Tyree. 1988. Mechanism of water stress-induced xylem embolism. *Plant Physiol.* 88:581–587.
- Sperry, J.S. and M.T. Tyree. 1990. Water-stress-induced xylem embolism in three species of conifers. *Plant Cell Environ.* 13:427–436.
- Sperry, J.S. and J.E.M. Sullivan. 1992. Xylem embolism in response to freeze-thaw cycles and water stress in ring-porous, diffuse-porous and conifer species. *Plant Physiol.* 100:605–613.
- Sperry, J.S. and N.Z. Saliendra. 1994. Intra- and inter-plant variation in xylem cavitation in *Betula occidentalis*. *Plant Cell Environ.* 17:1233–1241.
- Sperry, J.S. and U.G. Hacke. 2004. Analysis of circular bordered pit function. I. Angiosperm vessels with homogenous pit membranes. *Am. J. Bot.* 91:369–385.
- Sperry, J.S., A.H. Perry and J.E.M. Sullivan. 1991. Pit membrane degradation and air-embolism formation in ageing xylem vessels of *Populus tremuloides* Michx. *J. Exp. Bot.* 42:1399–1406.
- Sperry, J.S., K.L. Nichols, J.E.M. Sullivan and S.E. Eastlack. 1994. Xylem embolism in ring-porous, diffuse-porous, and coniferous trees of northern Utah and interior Alaska. *Ecology* 75:1736–1752.
- Sperry, J.S., U.G. Hacke and J.K. Wheeler. 2005. Comparative analysis of end wall resistivity in xylem conduits. *Plant Cell Environ.* 28:456–465.
- Tibbetts, T.J. and F.W. Ewers. 2000. Root pressure and specific conductivity in temperate lianas: exotic *Celastrus orbiculatus* (Celastraceae) versus native *Vitis riparia* (Vitaceae). *Am. J. Bot.* 87:1272–1278.
- Tyree, M.T., S.D. Davis and H. Cochard. 1994. Biophysical perspectives of xylem evolution—is there a tradeoff of hydraulic efficiency for vulnerability to dysfunction? *IAWA J.* 15:335–360.
- Wheeler, J.K., J.S. Sperry, U.G. Hacke and N. Hoang. 2005. Intervessel pitting and cavitation in woody Rosaceae and other vesselled plants: a basis for a safety versus efficiency trade-off in xylem transport. *Plant Cell Environ.* 28:800–812.
- Zimmermann, M.H. 1983. Xylem structure and the ascent of sap. Springer series in wood science. Ed. T.E. Timell. Springer-Verlag, Berlin, 143 p.
- Zimmermann, M.H. and C.L. Brown. 1977. *Trees: structure and function*. Springer Verlag, New York, 336 p.
- Zimmermann, M.H. and A.A. Jeje. 1981. Vessel length distribution of some American woody plants. *Can. J. Bot.* 59:1882–1892.
- Zimmermann, M.H. and D. Potter. 1982. Vessel length distribution in branches, stem, and roots of *Acer rubrum*. *IAWA Bull.* 3:103–109.